New generation of IWM-corner

Traction and braking power density and efficiency roadmap

Jurij Kern, Blaž Grafenauer, dr. Martin Strojnik, Stefano Guerra, dr. Gorazd Gotovac

Elaphe propulsion technologies, Inc., Ljubljana, Slovenia

E-mail: jurij.kern@elaphe-ev.com

ABSTRACT: The research presented in the paper evaluates the potential improvements to the traction and braking power density and efficiency in an in-wheel corner. While today's in-wheel motors can be used in a variety of applications, there is still a significant potential for improvement through control, thermal management and integration. Increasing performance, without adding mass and cost, is an important aspect of this disruptive development and will not only be useful for the high-performance applications, but applies equally, with different optimization, to mass market IWM applications. While the current solution and near-term solutions significantly improve on the previous generation of in-wheel motors the research also shows a path to achieve the target of 55 Nm/kg and more than 95% average highway efficiency.

KEY WORDS: in-wheel motor, power density, torque density, efficiency

1. INTRODUCTION

The advancement of modern automotive technologies requires innovative solutions to enhance vehicle utility, performance, safety, and comfort. Elaphe's in-wheel motor (IWM) technology (Fig. 1) presents an opportunity to design a new, control-centric vehicle platform by superior energy efficiency, packaging, faster control and new control degrees of freedom. At the same time IWM is controversial in a large part due to the additional unsuspended mass and related expected negative effects on ride dynamics, due to performance limitations in the limited space available in the wheel and due to a direct cost comparison with conventional e-axle solutions. Other work shows how direct drive in-wheel motor control aspects can be used to over-compensate the comfort and performance effects of additional unsprung mass and enhance vehicle riding experience (1).

The aim of this paper is to demonstrate how a new generation of in-wheel motors will be able to remove any remaining performance limitations, reduce the unsprung mass and allow in-wheel motors to be used in a variety of vehicles, opening the doors for new vehicle platforms that ultimately provide better efficiency, safety and user experience at lower cost.

A key role in this research is placed to longitudinal performance capabilities of an IWM-corner. This includes both traction and braking performance, where the front corners of the vehicle put more emphasis on braking and the rear put more emphasis on traction. The research focuses on control aspects, thermal aspects and integration aspects of the IWM corner solution and the tradeoffs between them.

The aspects of research and their impact are presented on a case of a front IWM-corner for high-performance vehicles. Such an application requires high braking performance and at the same time a light and powerful traction function with fast response time. The continuous power requirement is driven by a desire to be able to predictably induce significant amounts of yaw moment also at higher speeds. The technological advancements developed in such a system is however applicable widely for passenger car applications enhancing safety and user experience.

Fig. 1 Standard Elaphe direct drive motor layout with integrated friction brake

The research in this paper uses a High performance Elaphe in-wheel system (2024) as a baseline product for investigation, delivering 58 Nm/kg of maximum torque, 3.1 kW/kg of continuous power and 95% peak system efficiency within a 21'' standard automotive rim.

2. SYSTEM LEVEL OPTIMIZATION

2.1. E-motor control

Control significantly influences the e-motor design optimization. Both power density and efficiency are addressed by reducing overall e-motor and inverter losses. Two major e-motor aspects can be addressed by control:

- Motor constant ($T/\sqrt{P_{Cu}}$)
- Frequency losses in active materials

To address the motor constant we can take a look into torque equation of electric motor based on flux linkages $\psi_{d,q}$ in the d-q reference frame, where torque can be expressed as

$$M_{el} = \frac{3}{2} \cdot P_p \cdot [\psi_d \cdot i_q - \psi_q \cdot i_d]$$

with P_p as number of pole pairs, and $i_{d,q}$ are motor currents in d-q reference frame. Flux linkages are often simplified within linear first order model as a product between inductance and current as,

$$\psi_q = L_q i_q$$

while ψ_d additionally incorporates magnetic flux ψ_m,

$$\psi_d = L_d i_d + \psi_m$$

however in general, the flux linkages

$$\psi_{d,q} = f(i_d, i_q, T, \theta_{el})$$

are functions of both current components, motor temperatures T (not only of magnets but also rotor and stator, which affect airgap size), and importantly also of rotor position/angle θ_{el}. While currents and temperatures determine the average flux linkage value, position variation results in torque ripple, typically mostly associated with higher harmonics of electrical frequency.

Since an in-wheel motor cannot be mounted with vibration-damping elements, a significantly lower amount of torque ripple is required compared to a conventional centrally mounted e-motor. The torque ripple aspects are well analytically and numerically understood (4) and traditional reduction methods predominantly comprise the e-machine design – either by combination of stator and rotor pole pair numbers, magnet distribution or skewing of magnets or stator slots or magnet shape (2). While these methods are very effective in reducing the torque ripple, they also have a significant negative impact on the motor constant by lowering flux linkage (3). Instead, when the torque ripple amplitude can be reduced by control, significant gains in motor design can be obtained by increasing the flux linkage nominal values. Figures 2 b and d show an example of the torque output with and without magnet skewing, while 2a and c show corresponding phase currents with different control strategies. Since the stator geometry is the same we can get a direct comparison between currents, torques, and motor constant, as shown in Table 1. By implementing magnet skewing into motor design, we get in the presented operational point average torque of 462 Nm with 8 Nm of ripple (peak to peak value). Since the ripple is small, we see that different current controls in Figure 2a are very similar. On the other hand, if we omit the skewing, mean

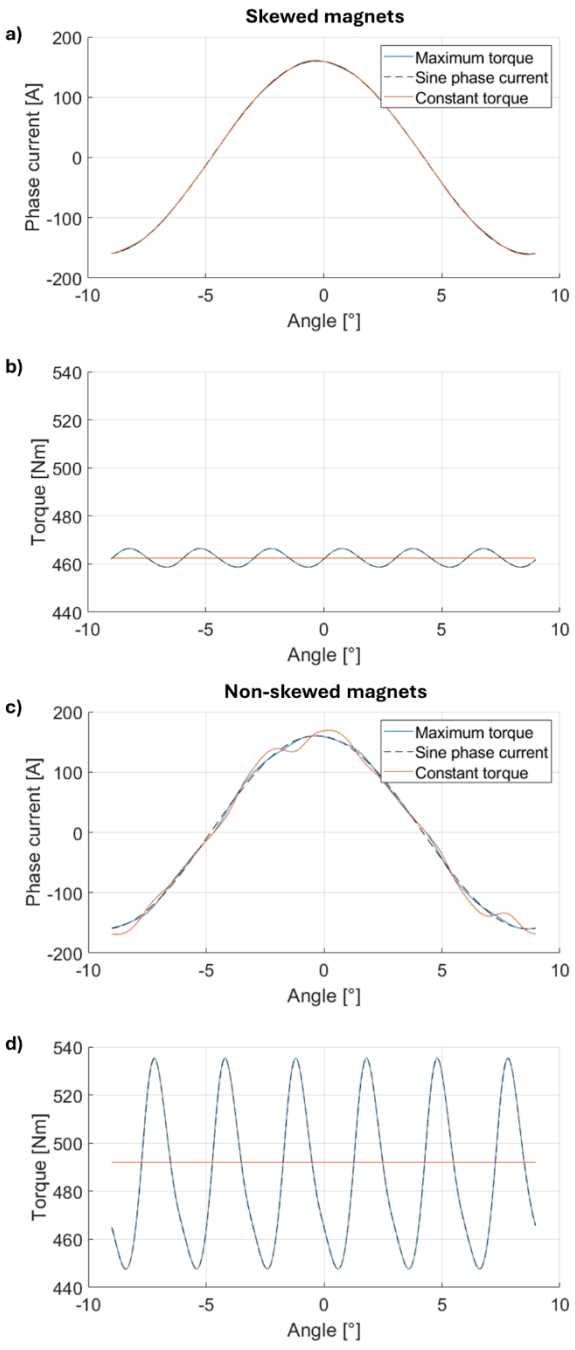

Fig. 2 Theoretical phase current shapes for a machine (a) with and (c) without HW ripple compensation. Next to intrinsic sinusoidal phase current also constant torque (or torque ripple compensation) current and maximum torque phase current shape are presented. On the plots (b) and (d) torque profiles for different phase currents are presented respectively.

torque is raised by 5% with the same sinusoidal current control, however the ripple is increased significantly to 88 Nm. By utilizing the constant torque control, it is possible to eliminate this torque by superimposing periodic current with current ripple

Table 1: Theoretical comparison of average torque output at constant RMS current for an Elaphe motor, utilizing rotor with skewed and non-skewed magnet configuration, at different control strategies. Additional to sinusoidal current control, minimum torque ripple and maximum torque controls are presented.

	phase current RMS [A]	total current ripple +/- [A]	mean torque [Nm]	torque ripple +/- [Nm]	torque constant [Nm/A]	motor constant [a.u.]
			SKEWED MAGNETS			
sin phase current	113,14	0,00	462,5	3,9	4,09	1
min torque ripple	113,15	1,51	462,5	0,0	4,09	1,00
max torque	113,14	0,00	462,5	3,9	4,09	1,00
			NON-SKEWED MAGNETS			
sin phase current	113,14	0,00	486,1	43,8	4,30	1,05
min torque ripple	113,29	15,83	486,3	0,0	4,29	1,05
max torque	113,14	0,00	486,3	43,9	4,30	1,05

amplitude of +-15,8 A, with negligible effect on RMS current, as can be seen from Table 1. The concrete improvement in the specific design is around 5%, depending on specific machine design, and amount of intrinsic ripple reduction within the machine, it can also grow up to 10%. Additionally, we see that while it is also possible to control the current in a way that we maximize the torque output with fixed RMS current this strategy brings negligible change to initial sinusoidal current control, and it is not beneficial for the specific investigated Elaphe in-wheel motor.

2.2. Power electronics topology

As motor torque and power density are pushed to the limits, typically the winding inductance will decrease. While that has a positive impact on the e-machine power factor, it will negatively influence the current ripple and result in frequency losses (4). As the inductance and losses are frequency dependent, simply raising switching frequency has limited benefit, moreover it also increases inverter losses, not necessarily contributing to higher system efficiencies.

Frequency losses can then be reduced by conventional methods, such as segmentation or finer lamination of parts, or splitting the wire into smaller threads. In typical machines, segmenting and laminating iron and magnet components has further distinctive effect, as it does not only reduces eddy currents inside the machine due to current ripple, but it also reduces current ripple itself, due to smaller decrease of inductance at high frequencies, as shown in figure 3, where we are comparing relative change of inductance between two machines, one with laminated rotor components and one without lamination. At low frequencies on the order of machine electrical frequencies, the inductance remains nearly constant, while at PWM frequencies there is a distinctive difference.

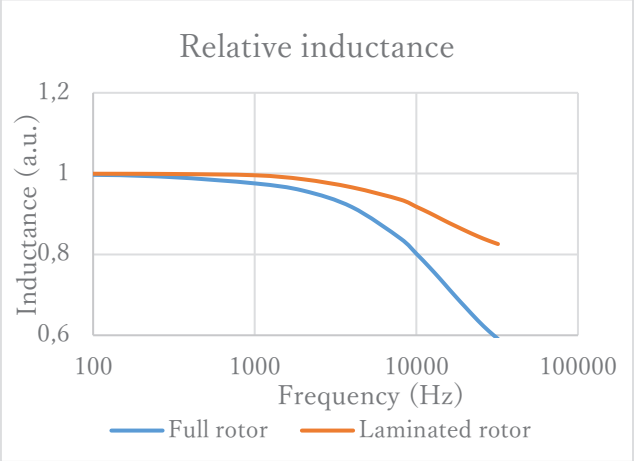

Figure 3: Frequency dependent inductance of machine with laminated and nonlaminated rotor components.

However, lamination and segmentation have negative consequences on power densities, through smaller effective material volume utilization, resulting in lower saturation, smaller effective magnet remanent field, lower amount of copper inside the slots, and finally worse cooling of the winding, all of which affect the final machine performance.

Cleaning up the current ripple allows the best combination of power density and efficiency (Figure 4). Even more distinctively,

for motors with distributed windings, where there is absence of low frequency harmonics in magnetic field inside the rotor, rotor losses are primarily induced by the current ripple, therefore reducing the current ripple has a relatively bigger impact on the rotor losses.

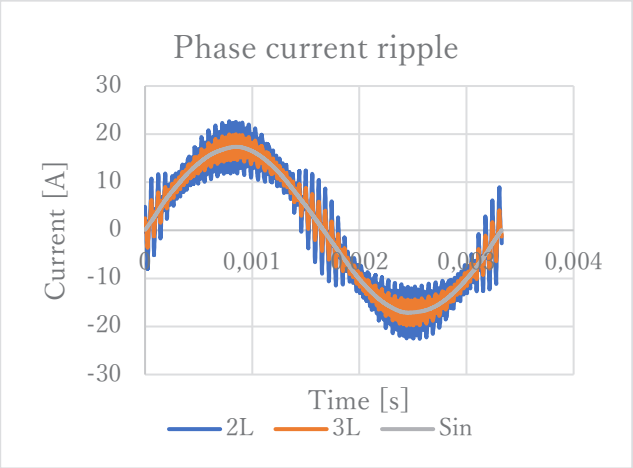

Figure 4: Simulated current ripple in a low torque, medium speed working point, with a 2-level inverter, 3-level inverter and purely sinusoidal excitation.

The full potential of removing the current ripple is seen in the exemplary consumption in table 2.

Table 2 Standard design WLTP average efficiency

	Baseline	**3-L inverter**	**Pure Sine system**
Power&torque density optimized machine	86%	90%	92%
Efficiency optimized machine	90%	91%	92%

Measurements with 3-L inverter confirm this effect showing an advancement in the efficiency map using the same e-machine, allowing 5-10 % increase in torque and power density without loss on efficiency.

2.2. Thermal management

A natural way to significantly improve power density and marginally improve cycle efficiency is to improve the heat removal. To optimize the system, different cooling methods have been analyzed to develop a roadmap of solutions.

To address the potential of the different solutions, first we must describe the relationship between the extracted heat and the cooling method. To start with we must consider the capability of the conduction of heat to the surface that is being cooled, expressed as

$$\frac{Q_{out}}{A} = \left(T_{hotspot} - T_{wall}\right) \cdot \lambda$$

where $\frac{Q_{out}}{A}$ is the extracted heat normalized per area, $T_{hotspot}$ is the temperature of the hottest point influencing performance, T_{wall} the temperature of the surface being cooled and λ the total thermal conductance between the hottest point influencing performance and the surface being cooled.

If we combine the equation above with the equation for heat transfer to a fluid, with the expression of the wall temperature

$$\frac{Q_{out}}{A} = \left(T_{wall} - T_{fluid}\right) \cdot HTC$$

$$T_{wall} = \frac{\frac{Q_{out}}{A}}{HTC} + T_{fluid}$$

where T_{fluid} is the bulk tempereature of the fluid to which the heat transfer coefficient HTC is normalized to, we get to the equation

$$\frac{Q_{out}}{A} = \frac{\left(T_{hotspot} - T_{fluid}\right) \cdot HTC \cdot \lambda}{(HTC + \lambda)}$$

Inserting relevant values for the Elaphe direct drive motor (as noted under *WEG jacket +* in Table 4) into the equation, it was found and later confirmed with FEA&CFD that without direct cooling, an improvement of 15% in continuous power and torque density can be achieved compared to a conventional water-glycol jacket, by connecting additional cooling elements to the cooled water jacket and thus providing additional heat transfer paths.

Some of the FEA results showing the most promising solution to shorten the thermal path can be observed on Figure 5, where the additional cooling element is placed above the motor end-windings. This results in a significant temperature drop of the hotspot, thus allowing roughly 32% more heat rejection at maximum operating conditions.

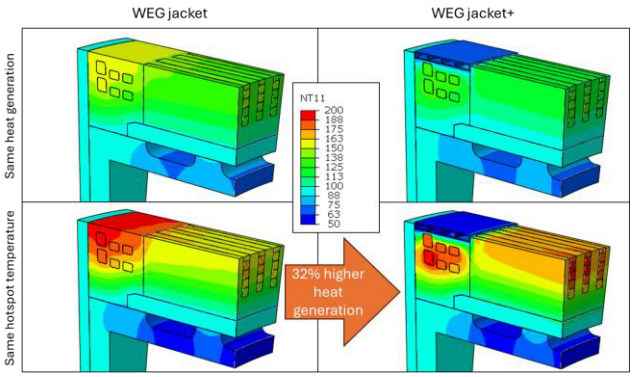

Figure 5 Temperature field from FEA comparing regular WEG jacket cooling to having additional cooling elements

The same approach can be used to evaluate the influence of direct cooling with a dielectric fluid to maximize thermal performance in special applications. Some of the properties influencing HTC for a dielectric fluid and 50%/50% WEG (water/ethylene glycol mixture) are shown below:

Table 3 Cooling fluid properties at 65°C

	WEG	Dielectric fluid	Units
Thermal conductivity	423	130	mW/m K
Specific heat	3460	2000	J/kg K
Density	1034	820	kg/m^3

We can observe that the combined factor of the ratio between both fluid properties is roughly 7, which assuming the same hydraulic power, same cooled surface temperature, same fluid flow conditions and same bulk fluid temperature, indicates that the HTC for the dielectric fluid is roughly 7-times lower compared to WEG. The benefit of cooling with a dielectric fluid, however, is that the fluid can be brough much closer to the main source of heat, the motor winding. An embodiment of the method of cooling where the motor end-windings are directly cooled with the dielectric fluid can be shown schematically as indicated on Figure 6.

When considering direct end-winding cooling however, the thermal path is significantly shorter and thus λ significantly greater. Therefore, despite the lower HTC value, when inserting the relevant values for the Elaphe direct drive motor (as noted under *Dielectric fluid* in Table 4) into the equation for $Q_{\frac{out}{A}}$, assuming the cooled area is of the same size for both cooling options, we calculate a 147% increase in cooling capability, which translates to roughly a 57% increase of the motor continuous power density in comparison to a regular WEG jacket cooling.

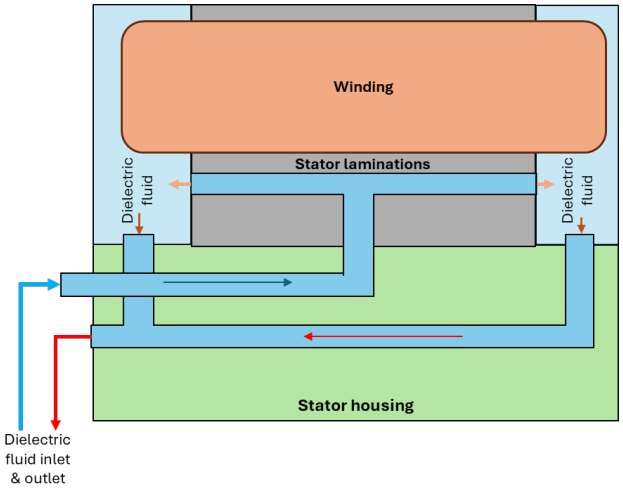

Figure 6 Schematics of motor end-winding direct cooling with a dielectric fluid

Table 4 Parameters for an Elaphe direct drive motor to be considered in the equation for $Q_{\frac{out}{A}}$ for different cooling methods

	WEG jacket	WEG jacket +	Dielectric fluid	Units
Total thermal conductance	227	300	1187	W/m^2 K
Relative HTC	7	7	1	/
$T_{hotspot}$	180	180	180	°C
T_{fluid}	65	65	65	°C

2.3 Braking function integration

While the traction function is important for a front IWM corner, the braking function requirement satisfaction is essential. Braking distance reduction potential if a vehicle is equipped with in-wheel motors, due to control advantages has been studied (6), but friction brake cooling in edge scenarios remains an important aspect for IWM solution scalability. Due to weight transfer and related tire-road contact patch forces, typically the braking torque in the front exceeds the traction force by a factor of 3 and more. The tight integration space and the thermal management of the friction brake traditionally limit the applicability of in-wheel motors for high-performance applications, as indicated in Figure 7.

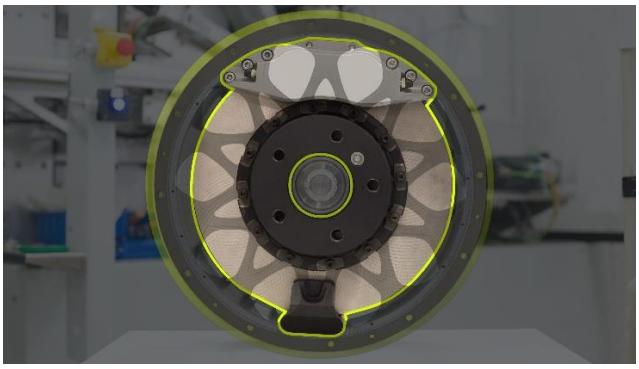

Figure 7 Overlayed picture of a mechanical brake integration into an in-wheel motor, indicating the tight integration space

However, a combination of a compact e-motor design, use of regenerative braking, use of out-of-phase braking and e-machine design with a ventilated rotor allow a significantly higher overall braking performance in the same wheel size.

The total braking power that is acting on the wheel P_{wheel} of an electric vehicle can be described with the equation below:

$$P_{wheel} = P_{el.mot} + P_{mech.brake} = \omega \cdot (T_{el.mot} + T_{mech.brake})$$

where $P_{el.mot}$ & $T_{el.mot}$ are the braking power & torque coming from the electric motor, $P_{mech.brake}$ & $T_{mech.brake}$ the braking power coming from the mechanical brake and ω the angular velocity of the wheel.

Since the electric motor is power limited and the mechanical brake is torque limited, the ratio between the two braking torques cannot be constant to fully exploit the benefits of an EV and a type of brake blending control algorithm must be introduced. Additionally, with motor control not only regenerative braking with the motor can be achieved but also out-of-phase braking (motor regeneration with intentionally lower efficiency, meaning that part of or the whole electric motor power is converted to losses in the motor), for situations where the battery is either full or thermally limited and the motor is not.

An example of the out of phase braking operation can be seen on measurements in Figure 8, which were performed on an Elaphe direct drive motor. From the measurements we can see that all the mechanical power being generated by the motor, at roughly 84 seconds into the measurement, starts being dissipated into heat and the motor heating up, while no power is being generated on the DC side. With this method, up to 8 kW can be dissipated by each IWM continuously and even up to 30 kW for short periods of time by each motor.

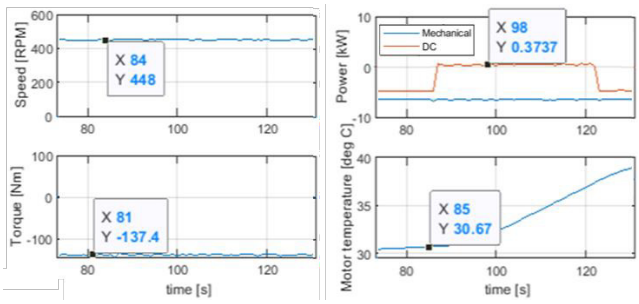

Figure 8: Measurements of an Elaphe motor during out-of-phase braking

The limit to out-of-phase braking is however that its continuous applicability is dictated solely by the heat dissipation capability of the motor (thus the importance of thermal management improvements described in the previous section). In a practical sense, this means that for braking events during for instance track driving, a smart brake blending control algorithm can optimally divide the request for the braking power based on the capability and thermal status of each component of the system, from the motor, power electronics, mechanical brake to the battery.

We can also split the power coming from the electric motor to:

$$P_{el.mot} = P_{el.mot\ reg} + P_{el.mot\ oop}$$

where $P_{el.mot\ reg}$ is the regenerative braking power and $P_{el.mot\ oop}$ is the out-of-phase braking power. Depending on the capability of the system, different $P_{el.mot}$ can be achieved and the requirements for the mechanical brake size can be influenced as shown on Figure 9. As an example, over 5 kg of disc weight can be saved, when 50 kW or more regeneration is available per front wheel.

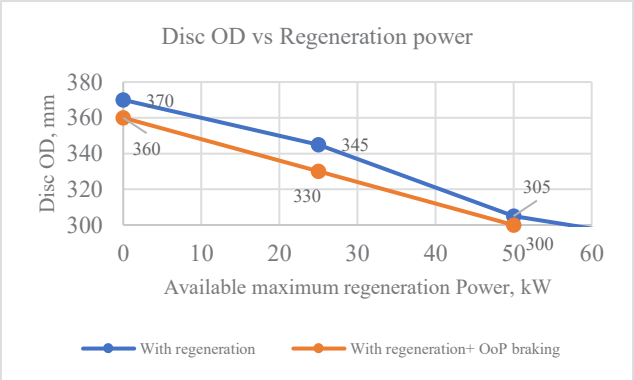

Figure 9 Brake disc sizing with different available regeneration power or with added 10kW of continuous out-of-phase braking power

3. CONCLUSIONS

Summarizing all the investigating solutions, the roadmap shows the ability to improve the power and torque density of the baseline machine by 10-20% when implementing control and power electronics topology to tailor the input current harmonics for torque smoothness and energy efficiency. An additional 15% improvement can be found by improving the thermal paths, leading to a 25-30% overall improvement in torque and power denistiy. The original machine can thus be built with 25-30% less active part mass, leading to a saving of 10-15% on the housing parts, which is cost effective as well as results in a lighter e-machine for the same performance.

Finally, if direct cooling is implemented in the target in-wheel motor system, the overall improvement is even much larger – with 60% reduction of the original active mass for the same continuous performance. Of course this is applicable only in some applications, since this course of action reduces efficiency and peak torque.

Using the proposed roadmap improvements, the conclusion of the research leads us to a roadmap of solutions that increasingly improve the output of the front IWM-corner reaching 76 Nm/kg torque density, 4 kW/kg power density and remaining with 95% average long distance driving efficiency.

If the system is set up properly with regards to the braking performance, the brake can be significantly reduced, further offsetting the added system weight by order of magnitude 5 kg in the front wheels or even eliminating the brake in the rear altogether.

When implemented to high performance vehicles, with higher vehicle speed requirements, all the improvements lead to 8 kW/kg of continuous power density while still achieving up to 95% average efficiency in long distance driving.

In the meantime, the available solutions continue to approach these numbers and break barriers of what applications can be realized with a control-centric vehicle architecture with in-wheel motors (Figure 10).

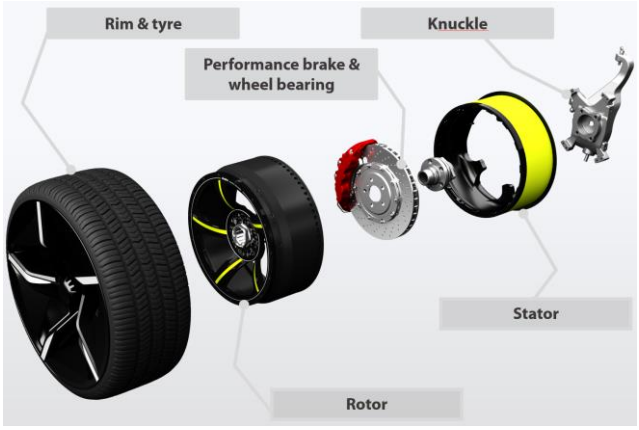

Figure 10 Optimized Elaphe direct drive motor for front corner of high- performance vehicle

REFERENCES

(1) Gotovac, G., Munih, G., Kompara, T., Brglez, L., Rucigaj, A., “Using high-bandwidth direct-drive architecture for new motion control capabilities”, Chassis.Tech Plus 2024, June 4-6th, 2024, Munich, Germany

(2) Gotovac, G., Miljavec, D., and Lampič, G., *Magn. IEEE Trans*, Analytical Model of Permeance Variation Losses in Permanent Magnets of the Multipole Synchronous Machine, vol. 49, 2, pp. 921–928.

(3) Richnow, J., Gerling, D., & Stenzel, P, “Torque ripple reduction in permanent magnet synchronous machines with concentrated windings and pre-wound coils”, *2014 17th International Conference on Electrical Machines and Systems (ICEMS),* pp 2501-2507, Oct. 22-25, 2014, Hangzhou, China

(4) Van der Geest, M., Polinder, H., & Ferreira, J. A. , “Influence of PWM switching frequency on the losses in PM machines”, *2014 International Conference on Electrical Machines (ICEM),* pp 1243-1247, 2-5 September 2014, Berlin, Germany

(5) Gotovac, G., Cogging Torque Elimination by Magnet Shaping in an In-wheel Motor, *21st Workshop on Rare-Earth Permanent Magnets and their Applications*, 29 August - 2 September 2010, Bled, Slovenia

(6) Modic B., Skrt U., Motaln, T., Lampič G., Gotovac, G., In-wheel powertrain functions for the autonomous and connected future, *EVS 31 & EVTeC 2018*, Kobe, Japan, October 1 - 3, 2018